Advances in Science and Technology Research Journal

Advances in Science and Technology Research Journal, 2026, 20(8), 146–162
https://doi.org/10.12913/22998624/220957
ISSN 2299-8624, License CC-BY 4.0

Received: 2026.03.26
Accepted: 2026.06.01
Published: 2026.07.01

Finite element analysis of the dynamic response of a functionally graded beam subjected to a two-degrees-of-freedom vehicle

Ba Thang Phung[1], Dang Diem Nguyen[2], Ngoc Tien Dao[3], Van Dat Pham[3*]

[1] University of Transport Technology, Hanoi, Vietnam
[2] University of Transport and Communications Campus in Ho Chi Minh, Vietnam
[3] Faculty of Civil Engineering, Hanoi Architectural University, Hanoi, Vietnam
* Corresponding author's e-mail: datpv@hau.edu.vn

ABSTRACT

This study investigated the vibration response of a functionally graded beam subjected to a two-degree-of-freedom moving load using the finite element method. The finite element formulations for the dynamic analysis of the classical functionally graded beam were derived based on Hamilton's variational principle. A MATLAB program was developed to compute the vibration response employing the Wilson–θ numerical integration algorithm. In addition, a semi-analytical solution was established to validate the finite element results proposed in this study. The comparison results demonstrate excellent agreement between the finite element method and the semi-analytical approach in predicting the vibration response of a beam. Parametric studies with various input conditions clearly reveal the significant influence of the load magnitude and load velocity on the dynamic behavior of the system. Furthermore, the results indicate that the dynamic amplification factor increases markedly along with velocity. Unlike previous FEM studies using simplified moving loads, this work explicitly formulated the coupled mass, damping, and stiffness matrices including Coriolis and centrifugal effects for a 2-DOF vehicle–FGM beam system.

Keywords: dynamics, FGM beam, FEM, moving vehicle.

INTRODUCTION

In recent decades, the dynamic behavior of structures subjected to moving loads has attracted widespread attention and become a core subject in structural mechanics. The rapid development of high-speed railway systems, large-span overpasses, and spatial structures requires engineers to possess accurate assessment tools for the complex vehicle-structure interaction. Numerous fundamental studies have focused on the dynamic response of structures under moving loads with constant or variable velocities [1–4]. In the early stages, the vehicle was often simplified as a moving point load. However, as the traveling speed increases, this model reveals significant limitations. Expanding the model to a moving mass problem – accounting for inertial, Coriolis, and centrifugal forces – has demonstrated the capability to more authentically capture the dynamic amplification factor. Furthermore, to accurately evaluate energy dissipation and vibration transmission, the vehicle system must be modeled as a moving oscillator incorporating mass, spring, and damper components [5, 6]. This complex interaction model provides profound insights into the resonance phenomenon, the effectiveness of which has also been proven when investigating structures with local defects [7] or nonlinear systems [8].

Parallel to the advancements in load modeling, the advent of functionally graded materials (FGMs) has revolutionized the design of structures subjected to dynamic loading. Unlike traditional laminated composites, which are prone to delamination due to stress concentration at the interfaces, FGMs possess the ability to continuously vary their mechanical properties over space. For FGM beams, the effective mass density and elastic modulus vary smoothly along the cross-sectional thickness, providing the structure with

both excellent bending stiffness and desired characteristics, such as wear resistance at the top surface and fracture toughness at the bottom [9–11]. These outstanding advantages have spurred a vast amount of research on the free vibration and natural frequency variation of FGM beams [12–16]. To accurately evaluate dynamic characteristics, various refined beam models have been developed and verified. Studies have indicated that for the FGM beams with a large thickness-to-length ratio or complex material gradients, the employment of higher-order shear deformation theories (HSDTs) or the Unified Formulation is imperative to replace the classical Euler-Bernoulli or Timoshenko theories [9–11, 16].

Beyond basic configurations, the research scope of FGM beams has been expanded to encompass the most complex geometric and microstructural variants. The modern theoretical framework has successfully addressed the vibration problems of axially FGM beams [17], curved beams [18], and tapered beams [19, 20]. At the micro-scale, size-dependent effects based on the nonlocal elasticity or modified couple stress theories have been integrated into nanobeams and microbeams [21, 22]. Notably, the load-bearing capacity of FGM can be outstandingly optimized by incorporating micro-porosities for weight reduction [23, 24], or by reinforcing the matrix with advanced materials, such as carbon nanotubes (CNTRCs) and functionally graded graphene platelets [25–27]. Researchers have also investigated the degradation of the overall system stiffness when beams operate under severe environmental conditions, such as hygrothermal fields [28, 29], or when interacting with complex foundation networks, such as a three-parameter viscoelastic foundation considering a bi-directional material gradient [30, 31].

To solve dynamic problems that account for the interaction between the structure and the moving load, numerical methods are generally required, as presented in the textbook [32, 33]. While refined analytical methods [14] and the dynamic stiffness method (DSM) [15] provide exact solutions serving as benchmarks, the finite element method (FEM) exhibits superior flexibility. FEM has successfully enabled the discretization and simulation of the dynamic response of non-uniform FGM beams [34, 35], porous beams under dynamic loads [23, 24], and paved the way for contemporary applications, such as piezoelectric energy harvesting systems [36, 37].

Beyond deterministic approaches, capturing the inherent randomness in material properties has emerged as a critical frontier in structural dynamics. Real-world functionally graded structures inevitably exhibit variations during manufacturing. Consequently, stochastic mechanics and uncertainty quantification have been employed to evaluate the free vibration of FGM plates with uncertain mass density [38]. This stochastic framework has been further advanced through stochastic higher-order finite element models for continuous beams resting on elastic supports with uncertain elastic moduli [39]. To achieve high-fidelity solutions for such complex systems, including bi-directional FGM sandwich beams partially supported by foundations [40], researchers have developed advanced computational tools, like the trigonometric enriched beam element for multi-phase materials [41], which are continually validated against rigorous exact analytical methods [42].

Although the literature on the dynamics of beams subjected to moving loads and FGM structures is remarkably extensive, the majority of prior studies remain confined to investigating homogeneous materials or applying overly simplified moving load models. The investigations delving into FGM beams subjected to a two-degree-of-freedom (2-DOF) moving vehicle using refined deterministic finite element methods are still highly limited. In particular, formulating a consistent element, establishing a system interaction matrix that accounts for the dynamics of the vehicle suspension system, and concurrently assessing the effects of moving speed and beam stiffness degradation on the dynamic amplification factor (DAF) represent a significant scientific gap that needs to be bridged.

Building upon the foregoing considerations, the present study aimed to develop a comprehensive mathematical and numerical modeling framework for evaluating the dynamic response of a functionally graded beam (FGB) subjected to a moving vehicle idealized as a two-degree-of-freedom (2-DOF) oscillator. The finite element formulation governing the coupled vehicle–structure interaction (VSI) was systematically derived employing Hamilton's variational principle, thereby ensuring a consistent representation of the inertial, elastic, and coupling effects inherent to the system. A purpose-built computational code was implemented within the MATLAB environment, wherein the transient response of the coupled system was advanced

incrementally in the time domain using the Wilson–θ implicit integration scheme [43]. This algorithm was selected owing to its favorable attributes of unconditional stability and high convergence rates in structural dynamics applications, and it remains widely adopted in contemporary studies addressing complex vehicle–structure interaction phenomena [44, 45]. Concurrently, a semi-analytical solution was developed to serve as a benchmark for validating the accuracy and reliability of the proposed finite element formulation. The findings of this investigation are anticipated to offer practical design insights for the deployment of functionally graded materials in next-generation bridge infrastructure and transportation systems, particularly under the scenarios involving dynamic vehicular loading. Beyond deterministic analyses, numerical optimization techniques have also been applied to reinforced concrete beams to identify optimal flexural strengthening strategies under various loading conditions [46–48].

Although the existing literature has addressed various aspects of FGM beams under moving loads, the majority of studies either simplify the moving vehicle as a moving mass or a single-degree-of-freedom oscillator, or employ analytical methods with limited applicability to complex boundary conditions and material distributions. To bridge this gap, the present study contributes the following novel elements: (i) a complete finite element formulation for the coupled vehicle–beam system that explicitly incorporates the time-dependent mass, Coriolis, and centrifugal matrices associated with the unsprung mass , which are often omitted in previous works; (ii) the systematic application of the Wilson–θ implicit time integration scheme to the coupled 2-DOF vehicle–FGM beam system, ensuring unconditional stability and accurate transient response; (iii) a comprehensive parametric investigation revealing, for the first time, the contrasting influence of suspension stiffness on the dynamic amplification factor as the sprung mass varies. Furthermore, recent advances in FGM beam dynamics under moving loads, including hygrothermal effects [28], viscoelastic foundations [30, 31], and energy harvesting applications [36, 37], have been incorporated into the literature review to better position the present work within the current state of the art.

FINITE ELEMENT FORMULATION

System description and kinematic assumptions

A functionally graded material (FGM) beam subjected to a moving vehicle idealized as a two-degree-of-freedom (2-DOF) oscillator was considered, as schematically depicted in Figure 1. The moving vehicle comprises two lumped masses, $m_1$and m_2, interconnected by a spring of stiffness k_s and a viscous damper with damping coefficient c [34]. The system translates along the beam axis at a constant forward speed v, maintaining continuous contact with the beam throughout its motion.

Consistent with classical Euler–Bernoulli beam theory, the displacement field is expressed as [34]:

$$U(x,z,t) = u(x,t) - z\frac{\partial w_b}{\partial x}$$
$$W(x,z,t) = w_b(x,t) \quad (1)$$

where: U and W denote the axial and transverse displacements, respectively [34].

The corresponding normal strain is given by:

$$\varepsilon_x = \frac{\partial U}{\partial x} = \frac{\partial u}{\partial x} - z\frac{\partial^2 w_b}{\partial x^2} = \varepsilon_x^0 + z\kappa_x^b \quad (2)$$

where: $\varepsilon_x^0 = \frac{\partial u}{\partial x}$ represents the membrane strain, $\kappa_x^b = -\frac{\partial^2 w_b}{\partial x^2}$ denotes the bending curvature.

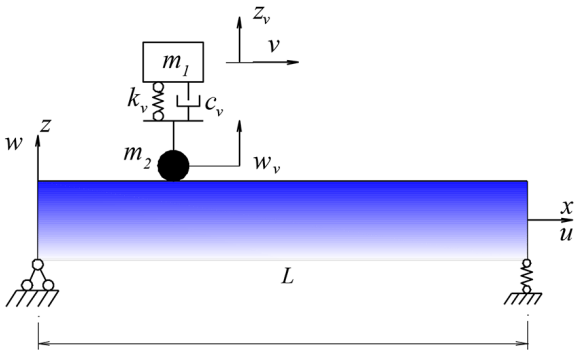

Figure 1. Schematic representation of a moving vehicle traversing an FGM beam

Material properties of the functionally graded beam

The beam is composed of ceramic and metallic phases, with material properties varying continuously across the thickness direction according to a power-law distribution. The effective elastic modulus $E(z)$ and mass density $p(z)$ at any point through the thickness are defined as [34]:

$$E(z) = (E_c - E_m)\left(\frac{z}{h} + \frac{1}{2}\right)^p + E_m;\ \rho(z) = \\ = (\rho_c - \rho_m)\left(\frac{z}{h} + \frac{1}{2}\right)^p + \rho_m \tag{3}$$

where: the subscripts m and c refer to the metallic and ceramic constituents, respectively; h denotes the beam thickness; and p is the non-negative power-law index governing the material gradation profile [35].

Finite element discretization

A two-node beam element with six degrees of freedom per element is employed [35]. The axial displacement is interpolated using linear shape functions, whereas the transverse deflection is approximated using Hermitian cubic polynomials to ensure C^1-continuity:

$$u(x,t) = N_1(x)u_1 + N_2(x)u_2; \\ w_b(x,t) = N_3(x)w_1 + N_4(x)\theta_1 + \\ +N_5(x)w_2 + N_6(x)\theta_2. \tag{4}$$

where: $\theta = \partial w_b / \partial x$ represents the rotational degree of freedom. The shape functions are explicitly expressed as:

$$N_1 = 1 - \frac{x}{L_e};\ N_2 = \frac{x}{L_e};\ +2\left(\frac{x}{L_e}\right)^3;$$

$$N_3 = 1 - 3\left(\frac{x}{L_e}\right)^2;\ N_4 = x\left(\frac{x}{L_e} - 1\right)^2; \tag{5}$$

$$N_5 = 3\left(\frac{x}{L_e}\right)^2 - 2\left(\frac{x}{L_e}\right)^3;\ N_6 = x\left[\left(\frac{x}{L_e}\right)^2 - \frac{x}{L_e}\right]$$

The element nodal displacement vector is defined as $\{\mathbf{u}_e\} = \{u_1, u_2, w_1, \theta_1, w_2, \theta_2\}^T$, and the displacement field within the element can be expressed in matrix form as [35]:

$$\begin{Bmatrix} u(x,t) \\ w_b(x,t) \end{Bmatrix} = \\ = \begin{bmatrix} N_1 & N_2 & 0 & 0 & 0 & 0 \\ 0 & 0 & N_3 & N_4 & N_5 & N_6 \end{bmatrix} \{\mathbf{u}_e\} \tag{6}$$

Element stiffness and mass matrices

The strain energy stored in the beam element is given by [35]:

$$U_e = \frac{1}{2}\int_{V_e} \sigma_x\, \varepsilon_x dV = \frac{1}{2}\int_0^{L_e} [\varepsilon_0 \quad \kappa] \\ \begin{bmatrix} A & -B \\ -B & D \end{bmatrix} \begin{bmatrix} \varepsilon_0 \\ \kappa \end{bmatrix} dx \tag{7}$$

where the sectional rigidities are defined as:

$$A = \iint_A E(z)\, dA;\ B = \iint_A zE(z)\, dA; \\ D = \iint_A z^2 E(z)\, dA \tag{8}$$

The kinetic energy of the element, accounting for both axial and flexural motions, is expressed as:

$$T = \frac{1}{2}\int_V \rho(z)\left\{\begin{matrix}\left(\dot{u} - z\dfrac{\partial \dot{w}_b}{\partial x}\right)^2 \\ +(\dot{w}_b)^2\end{matrix}\right\} dV \tag{9}$$

The associated inertia terms are defined as:

$$I_0 = \iint_A \rho(z) z^i dz;\ I_1 = \iint_A \rho(z) z dz; \\ I_2 = \iint_A \rho(z) z^2 dz \tag{10}$$

Substituting the displacement approximations into the energy expressions and applying Hamilton's principle yields (see Appendix) the element stiffness matrix $[K]_e$ and element mass matrix $[M]_e$, which are provided in Equations 11 and 12, respectively [45]. These matrices account for the coupling between axial and bending deformations arising from the material asymmetry when B ≠ 0:

$$[K]_e = \begin{bmatrix} \frac{A}{L_e} & -\frac{A}{L_e} & \frac{6B}{L_e^2} & \frac{4B}{L_e} & -\frac{6B}{L_e^2} & \frac{2B}{L_e} \\ & \frac{A}{L_e} & -\frac{6B}{L_e^2} & -\frac{4B}{L_e} & \frac{6B}{L_e^2} & -\frac{2B}{L_e} \\ & & \frac{12D}{L_e^3} & \frac{6D_{11}}{L_e^2} & -\frac{12D}{L_e^3} & \frac{6D_{11}}{L_e^2} \\ & & & 4L_e^2 & -\frac{6D_{11}}{L_e^2} & \frac{2D}{L_e} \\ & & & & & -\frac{6D_{11}}{L_e^2} \\ Sym & & & & & \frac{4D}{L_e} \end{bmatrix} \tag{11}$$

$$[M]_e = \begin{bmatrix} \frac{I_0 L_e}{3} & \frac{I_0 L_e}{6} & \frac{I_1 L_e}{6} & \frac{I_1 L_e^2}{12} & -\frac{I_1 L_e}{6} & -\frac{I_1 L_e^2}{12} \\ & \frac{I_0 L_e}{3} & \frac{I_1 L_e}{6} & \frac{I_1 L_e^2}{12} & -\frac{I_1 L_e}{6} & -\frac{I_1 L_e^2}{12} \\ & & \frac{156 I_0 L_e}{420} & \frac{22 I_0 L_e^2}{420} & \frac{54 I_0 L_e}{420} & -\frac{13 I_0 L_e^2}{420} \\ & & & \frac{4 I_0 L_e^3}{420} & \frac{13 I_0 L_e^2}{420} & -\frac{3 I_0 L_e^3}{420} \\ & & & & \frac{156 I_0 L_e}{420} & -\frac{22 I_0 L_e^2}{420} \\ Sym & & & & & \frac{4 I_0 L_e^3}{420} \end{bmatrix} \quad (12)$$

Equations of motion for the coupled vehicle–beam system

The dynamic equilibrium of the moving vehicle is governed by Newton's second law. For the sprung mass m_1, the equation of motion is expressed as [45]:

$$m_1 \ddot{z}_v + c_s(\dot{z}_v - \dot{w}_v) + k_s(z_v - w_v) = 0 \quad (13)$$

where: z_v denotes the vertical displacement of mass m_1, and $w_v = w(x_v, t)$ = represents the beam deflection at the instantaneous contact point. The interaction force transmitted to the beam comprises the static weight of the vehicle and the dynamic components arising from the motion of the unsprung mass m_2:

$$P_0 = (m_1 + m_2)g - m_2 \ddot{w}_v + F_{m1} \quad (14)$$

where: Fm_1 denotes the force transferred from the sprung mass to the unsprung mass through the suspension system:

$$F_{m1} = k(y - w_m) + c(\dot{y} - \dot{w}_m) = -m_1\, \ddot{y} \quad (15)$$

Upon assembly of the element contributions, the global equation of motion for the beam alone is obtained as [45]:

$$[M]\{\ddot{\boldsymbol{U}}\} + [K]\{\boldsymbol{U}\} = \{\boldsymbol{N}\}^T\{P_0\} \quad (16)$$

where: $[M]$ and $[K]$ are the global mass and stiffness matrices, respectively, and {N}is the vector of shape functions evaluated at the current load position [45]. Notably, the load vector is non-zero only for the element over which the moving vehicle resides at a given time instant.

Note that the load vector is non-zero only for the element in which the moving load is currently located.

By coupling the beam dynamics with the vehicle equations, the complete system governing the vehicle–structure interaction is expressed in a matrix form as:

$$\begin{bmatrix} [M] + [m]_{v2} & \{0\} \\ \{0\} & m_1 \end{bmatrix} \begin{Bmatrix} \ddot{\boldsymbol{U}} \\ \ddot{z}_v \end{Bmatrix} + \begin{bmatrix} [c]_{v2} & 0 \\ -c_s\{\boldsymbol{N}\} & c_s \end{bmatrix} \begin{Bmatrix} \dot{\boldsymbol{U}} \\ \dot{z}_v \end{Bmatrix} + \begin{bmatrix} [K] + [k]_{v2} & 0 \\ -c_s\dot{x}\frac{d\{\boldsymbol{N}\}}{dx} - k_s\{\boldsymbol{N}\} & k_s \end{bmatrix} \begin{Bmatrix} \boldsymbol{U} \\ z_v \end{Bmatrix} = \begin{bmatrix} \{\boldsymbol{N}\}^T(m_1 + m_2)g \\ 0 \end{bmatrix} \quad (17)$$

The auxiliary matrices introduced in Equation 17 account for the inertial, centrifugal, and Coriolis effects induced by the moving unsprung mass m_2, and are defined as:

$$[m]_{v2} = m_2\{\boldsymbol{N}\}^T\{\boldsymbol{N}\};$$

$$[c]_{v2} = 2m_2\dot{x}(t)\{\boldsymbol{N}\}^T\frac{d\{\boldsymbol{N}\}}{dx};$$

$$[k]_{v2} = m_2\dot{x}^2(t)\{\boldsymbol{N}\}^T\frac{d^2\{\boldsymbol{N}\}}{dx^2} + m_2\ddot{x}(t)\{\boldsymbol{N}\}^T\frac{d\{\boldsymbol{N}\}}{dx} + k\{\boldsymbol{N}\}^T\{\boldsymbol{N}\} + c\dot{x}(t)\{\boldsymbol{N}\}^T\frac{d\{\boldsymbol{N}\}}{dx}$$

These expressions encapsulate the time-dependent nature of the coupling between the moving vehicle and the deformable beam structure, thereby providing a complete framework for transient dynamic analysis.

To further justify the use of the two-degree-of-freedom (2-DOF) vehicle model, a brief comparison with simpler load models is warranted. The simplest representation, the moving point load, neglects all inertia effects of the vehicle and therefore cannot capture the dynamic interaction between the vehicle and the beam. The moving mass model accounts for the inertia of the unsprung mass but omits the suspension system, thereby failing to represent the filtering and phase-lag effects introduced by the spring and damper. In contrast, the 2-DOF oscillator model adopted herein incorporates both the sprung and unsprung masses, as well as the suspension stiffness and damping, enabling it to capture essential phenomena, such as vehicle bounce, energy dissipation,

and the phase lag that can reduce the dynamic amplification factor under certain conditions (see Section 'Influence of the moving load velocity'). For the parameter ranges considered in this study (vehicle speeds up to 30 m/s and suspension stiffness from 10^6 to 10^7 N/m), the moving point load overestimates the peak displacement by as much as 30% compared to the 2-DOF model, confirming that the additional complexity of the 2-DOF model is necessary for accurate predictions.

SOLUTION OF THE COUPLED EQUATIONS OF MOTION USING THE WILSON–Θ METHOD

To solve the coupled governing equations of motion derived in the preceding section, a step-by-step time integration procedure is required owing to the time-dependent nature of the vehicle–structure interaction. Among the various implicit integration schemes available in structural dynamics, the Wilson–θ method was employed herein due to its favorable stability characteristics and numerical accuracy for systems with time-varying parameters.

The global equations of motion for the coupled vehicle–beam system, as expressed in Equation 17, can be recast in the following compact matrix form [35]:

$$\left[\underset{\sim}{M}\right]\left\{\ddot{\underset{\sim}{u}}(t)\right\}+\left[\underset{\sim}{C}\right]\left\{\dot{\underset{\sim}{u}}(t)\right\}+ +\left[\underset{\sim}{K}\right]\left\{\underset{\sim}{u}(t)\right\}=\{P(t)\} \tag{18}$$

where: $[M]$, $[C]$, and $[K]$ denote the global mass, damping, and stiffness matrices of the coupled system, respectively; $\{u(t)\}$ represents the vector of unknown displacements, including both beam nodal degrees of freedom and the vehicle displacement; and $\{P(t)\}$ is the corresponding external force vector [45].

Formulation of the effective stiffness matrix

Within the framework of the Wilson–θ method, the solution proceeds by assuming a linear variation of the acceleration over an extended time step $\theta\Delta$, where $\theta \geq 1.37$ to ensure unconditional stability [35]. The effective stiffness matrix, which remains constant throughout the integration procedure for linear systems, is formulated as:

$$\left[\widehat{K}\right]=\left[\underset{\sim}{K}\right]+a_0\left[\underset{\sim}{M}\right]+a_1\left[\underset{\sim}{C}\right] \tag{19}$$

The integration constants appearing in Eq. (19) are defined as: $a_0=\frac{1}{\beta(\theta\Delta t)^2}$; $a_1=\frac{\gamma}{\beta\theta\Delta t}$

Following the standard implementation of the Wilson–θ algorithm, the parametersγ and β are selected as γ = 1/2 and β = 1/6 which correspond to a linear acceleration assumption within the extended time interval.

Effective force vector and solution procedure

The effective force vector at the extended time station $t + \theta\Delta$ is constructed from the known system states at time t and the prescribed external forces. This vector is expressed as [45]:

$$\left\{\widehat{P}(t+\theta)\right\}=\left[\underset{\sim}{M}\right]\begin{pmatrix}a_0\left\{\dot{\underset{\sim}{u}}(t)\right\}\\+a_1\left\{\dot{\underset{\sim}{u}}(t)\right\}\\+a_2\left\{\ddot{\underset{\sim}{u}}(t)\right\}\end{pmatrix}\{P(t)\}+\ldots +\theta(\{P(t+\theta)\}-\{P(t)\})+\left[\underset{\sim}{C}\right] \left(a_1\left\{\dot{\underset{\sim}{u}}(t)\right\}+a_4\left\{\dot{\underset{\sim}{u}}(t)\right\}+a_5\left\{\ddot{\underset{\sim}{u}}(t)\right\}\right) \tag{20}$$

where the auxiliary integration constants are given by: $a_2=\frac{1}{\beta\theta\Delta t}; a_4=\frac{\gamma}{\beta}-1; a_5=\left(\frac{\gamma}{\beta}-2\right)\frac{\theta\Delta t}{2}$

Upon assembly of the effective stiffness matrix and the effective force vector, the displacement solution at the extended time step is obtained by solving the system of linear algebraic equations [35]:

$$\left[\underset{\sim}{K}\right]\left\{\underset{\sim}{u}(t+\theta)\right\}=\left\{\widehat{P}(t+\theta)\right\} \tag{21}$$

Computation of acceleration, velocity, and displacement

Once the displacements at time $t + \theta\Delta$ are determined, the corresponding acceleration vector is evaluated as [45]:

$$\left\{\ddot{\underset{\sim}{u}}(t+\theta)\right\}=a_0\left(\left\{\underset{\sim}{u}(t+\theta)\right\}-\left\{\underset{\sim}{u}(t)\right\}\right)- -a_2\left\{\dot{\underset{\sim}{u}}(t)\right\}-\left(\frac{1}{2\beta}-1\right)\left\{\ddot{\underset{\sim}{u}}(t)\right\} \tag{22}$$

Since the Wilson–θ method employs an extended time step for prediction, the acceleration at the actual time step $t + \Delta t$ is obtained through linear interpolation between the known acceleration at time t and the computed acceleration at time $t + \theta\Delta$ [35]:

$$\begin{aligned}
\left\{\ddot{u}(t+\Delta t)\right\} &= \{\ddot{u}(t)\} + \\
&+\frac{1}{\theta}\left(\left\{\ddot{u}(t+\theta)\right\} - \left\{\ddot{u}(t)\right\}\right); \\
\left\{\dot{u}(t+\Delta t)\right\} &= \left\{\dot{u}(t)\right\} + \\
&+ (1-\gamma)\Delta t\left\{\ddot{u}(t)\right\} + \\
&\gamma\Delta t\left\{\ddot{u}(t+\Delta t)\right\}; \\
\left\{u(t+\Delta t)\right\} &= \left\{u(t)\right\} + \Delta t\left\{\dot{u}(t)\right\} + \\
&+\left(\frac{1}{2}-\beta\right)\Delta t^2\left\{\ddot{u}(t)\right\} + \beta\Delta t^2\left\{\ddot{u}(t+\Delta t)\right\}
\end{aligned} \tag{23}$$

The recurrence scheme defined by Eq. (23) allows for the stepwise propagation of the solution in the time domain, commencing from the prescribed initial conditions. The algorithm was implemented in the MATLAB environment, enabling efficient computation of the transient dynamic response of the coupled vehicle–beam sy stem.

SEMI-ANALYTICAL FORMULATION FOR VALIDATION

To verify the accuracy of the finite element formulation presented in Section 2, a semi-analytical solution was developed in this section. This approach serves as an independent benchmark, enabling rigorous validation of the numerical results obtained from the coupled vehicle–beam finite element model.

Governing differential equations

Based on the classical Euler–Bernoulli beam theory, the equations governing the forced vibration of a functionally graded beam subjected to a moving point load can be derived from the equilibrium of internal forces and external loading. The axial force and bending moment resultants are defined as [45]:

$$\begin{aligned}
N &= \iint_A \sigma_x\, dA = A\varepsilon_x^0 + B\kappa_x^b; \\
M &= \iint_A z\sigma_x\, dA = B\varepsilon_x^0 + D\kappa_x^b
\end{aligned} \tag{24}$$

where: $\varepsilon_x^0 = \frac{\partial u}{\partial x}$ and $\kappa_x^b = -\frac{\partial^2 w_b}{\partial x^2}$. The sectional rigidities A, B, and D have been previously defined in Equation 8. Incorporating these resultant expressions into the equations of motion yields the following coupled differential equations:

$$\begin{aligned}
&\frac{\partial N}{\partial x} = I_0\ \ddot{u} - I_1\ \frac{\partial \ddot{w}_b}{\partial x}; \\
&\frac{\partial^2 M}{\partial x^2} + P_0\delta(x-vt) = \\
&= I_0\ \ddot{w}_b + I_1\ \frac{\partial \ddot{u}}{\partial x} - I_2\ \frac{\partial^2 \ddot{w}_b}{\partial x^2}
\end{aligned} \tag{25}$$

Substituting the internal force expressions from Equation 24 into Equation 25 leads to the following system of partial differential equations expressed in terms of the axial displacement $u(x,t)$ and transverse displacement $w_b(x,t)$ [45]:

$$\begin{aligned}
&A\frac{\partial^2 u}{\partial x^2} - B\frac{\partial^3 w_b}{\partial x^3} = I_0\ \ddot{u} - I_1\ \frac{\partial \ddot{w}_b}{\partial x}; \\
&B\frac{\partial^3 u}{\partial x^3} - D\frac{\partial^4 w_b}{\partial x^4} + P_0\delta(x-vt) = \\
&= I_0\ \ddot{w}_b + I_1\ \left(\frac{\partial \ddot{u}}{\partial x}\right) - I_2\ \frac{\partial^2 \ddot{w}_b}{\partial x^2}
\end{aligned} \tag{26}$$

It is noteworthy that the coupling between axial and flexural responses arises from the material asymmetry characterized by the B term, which is non-zero when the material properties are not symmetric about the neutral axis [45].

Modal discretization using trigonometric shape functions

To obtain a semi-analytical solution, the displacement fields were approximated using a single-mode expansion that satisfies the simply supported boundary conditions. Specifically, the axial and transverse displacements were assumed to take the following forms:

$$\begin{aligned}
u(x,t) &= U_{sem}(t)\cos\left(\frac{\pi}{L}x\right) \\
w_b(x,t) &= W_{sem}(t)\sin\left(\frac{\pi}{L}x\right)
\end{aligned} \tag{27}$$

These assumed modes satisfy the essential boundary conditions for a simply supported beam, namely $w_b = 0$ and $\partial^2 w_b / \partial x^2 = 0$ at $x = 0$ and $x = L$, as well as the natural boundary conditions for axial motion [45].

Substituting the displacement approximations from Equation 27 into the governing Equation 26 yields the following residual expressions.

- For the axial equilibrium equation:

$$\begin{aligned} &-AU_{sem}(t)\left(\frac{\pi}{L}\right)^2 \cos\left(\frac{\pi}{L}x\right) + \\ &+ BW_{sem}(t)\left(\frac{\pi}{L}\right)\cos\left(\frac{\pi}{L}x\right) = \\ &= I_0\ \ddot{U}_{sem}(t)\cos\left(\frac{\pi}{L}x\right) - \\ &-I_1\ \ddot{W}_{sem}(t)\left(\frac{\pi}{L}\right)cos\left(\frac{\pi}{L}x\right) \end{aligned} \tag{28}$$

- For the transverse equilibrium equation:

$$\begin{aligned} &BU_{sem}(t)\left(\frac{\pi}{L}\right)^3 \sin\left(\frac{\pi}{L}x\right) - \\ &DW_{sem}(t)\left(\frac{\pi}{L}\right)^4 \sin\left(\frac{\pi}{L}x\right) + P_0\delta(x-vt) = \\ &= I_0\ \ddot{W}_{sem}(t)\sin\left(\frac{\pi}{L}x\right) - \\ &\ddot{U}_{sem}(t)\left(\frac{\pi}{L}\right)\sin\left(\frac{\pi}{L}x\right) - I_2\ \ddot{W}_{sem}\left(\frac{\pi}{L}\right)^2 \sin\left(\frac{\pi}{L}x\right) \end{aligned} \tag{29}$$

Reduction to ordinary differential equations

The orthogonality properties of the trigonometric functions over the domain $[0, L]$ were exploited to eliminate the spatial dependence. Specifically, multiplying Equation 28 by $\cos(\pi x/L)$ and Equation 29 by $\sin(\pi x/L)$, followed by integration from 0 to L, yields a system of ordinary differential equations governing the time evolution of the generalized coordinates $U_{sem}(t)$ and $W_{sem}(t)$.

The resulting system can be expressed in the following compact matrix form [45]:

$$\begin{aligned} &[M_{sem}]\{\ddot{u}_{sem}(t)\} + [C_{sem}]\{\dot{u}_{sem}(t)\} + \\ &+[K_{sem}]\{u_{sem}(t)\} = \{P_{sem}(t)\} \end{aligned} \tag{30}$$

where: $\{u_{sem}(t)\} = \{U_{sem}(t), W_{sem}(t)\}^T$ is the vector of generalized displacements, $[M_{sem}]$ and $[K_{sem}]$ represent the generalized mass and stiffness matrices, respectively, while $[C_{sem}]$ accounts for any damping effects, if present. The generalized force vector $\{P_{sem}(t)\}$ arises from the moving load term $P_0\delta(x - vt)$ and incorporates the spatial distribution of the load through the integration with the mode shapes.

Time integration and validation

The system of ordinary differential equations defined in Equation 30 was solved numerically using the Wilson–θ time integration scheme, consistent with the approach employed for the finite element model described in Section 3. This consistency in the time integration method ensures that any discrepancies between the two models can be attributed solely to the spatial discretization strategies, rather than to the differences in the temporal solution algorithms.

The semi-analytical solution obtained from this procedure provides an efficient means for validating the finite element results. By comparing the dynamic responses predicted by both approaches under identical loading and boundary conditions, the accuracy and convergence characteristics of the proposed finite element formulation can be rigorously assessed.

NUMERICAL EXAMPLES AND PARAMETRIC STUDIES

This section presents numerical investigations to validate the proposed finite element formulation and to examine the dynamic response characteristics of functionally graded beams subjected to moving vehicle loads. Unless otherwise specified, the material properties and system parameters remain consistent with those defined in the validation study.

Model validation

To establish the accuracy of the finite element formulation developed in Section 2, a validation study is conducted by comparing numerical predictions with those obtained from the semi-analytical solution described in Section 4. A simply supported functionally graded beam of length L = 1 m is considered, with a rectangular cross-section of width b = 4 cm and thickness h = 8 cm. The material constituents comprise aluminum

(metal) and ceramic phases, with the following properties adopted from Ref. [45]:

- Young's modulus: E_m = 70 GPa (metal), E_c = 380 GPa (ceramic)
- Mass density: ρm = 2707 kg/m^3

The volume fractions follow a power-law distribution through the thickness as defined in Equation 3, with a gradient index of $p = 2$. The moving vehicle parameters are specified as m_1 = 100 kg, m_2 = 50 kg, suspension stiffness $k_v = 10^6$ N/m, damping coefficient $c_v = 10^4$ N · s/m and constant travelling speed v = 20 m/s [45].

Figure 2 presents a comparison of the mid-span displacement response as a function of the dimensionless load position parameter vt/L. The results obtained from the proposed finite element model were plotted alongside those from the semi-analytical solution. As illustrated in the figure, excellent agreement was observed between the two approaches, with only marginal discrepancies in the displacement amplitude. The maximum displacement occurs when the moving load traverses the beam mid-span, which is consistent with the expected dynamic behavior for simply supported beams. This close correlation confirms the validity and reliability of the finite element formulation, establishing a firm foundation for the subsequent parametric studies.

Parametric investigations

Building upon the validated finite element model, this subsection systematically examines the influence of key system parameters on the dynamic response of the functionally graded beam. To quantify the dynamic amplification effect, the impact factor (IF) is defined as [45]:

$$IF = \frac{v_{max}}{v_0} \tag{31}$$

where: v_{max} denotes the maximum mid-span displacement under dynamic moving load conditions, and v_0 represents the corresponding static displacement when the same load magnitude is applied at the mid-span [45].

Effects influence of the power-law index p

The effect of the material gradation parameter p on both the displacement response and the impact factor is illustrated in Figure 3. The results reveal that the power-law index significantly influences the structural dynamic behavior, primarily through its effect on the effective bending stiffness.

As it is shown in Figure 3(a), the dimensionless mid-span deflection increases monotonically with increasing p. For values of p = 1, 22, and 33, the peak deflection progressively rises, with the case p = 3 exhibiting a substantially larger deflection compared to p = 1. This trend is attributed to the increasing metallic volume fraction as p increases, which results in a reduction of the overall bending stiffness. Consequently, the beam exhibits diminished resistance to deformation under dynamic loading.

Figure 3(b) demonstrates that the impact factor increases nearly linearly with the power-law index over the range p = 1 to 55. This observation

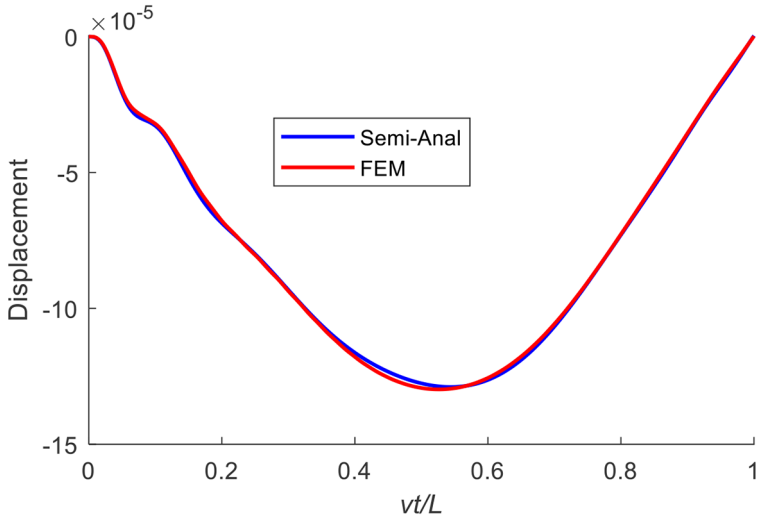

Figure 2. Comparison of mid-span beam displacement obtained by FEM and the semi-analytical solution

indicates that the dynamic amplification effect becomes more pronounced as the structural stiffness decreases. The stiffness degradation amplifies the vibration response, leading to greater dynamic magnification. Collectively, these results underscore the critical role of material gradation in governing the dynamic performance of functionally graded beams under moving loads.

Influence of the sprung mass m_1

Figure 4 examines the effect of the sprung mass m_1 on both the mid-span displacement and the impact factor. Figure 4(a) presents the displacement responses for three distinct values of m_1: 100 kg, 200 kg, and 300 kg. As anticipated, increasing the sprung mass elevated the total applied load, resulting in a corresponding increase in the displacement amplitude.

Figure 4(b) illustrates the variation of the impact factor as m_1 increases from 100 kg to 300 kg, considering two distinct suspension stiffness values, namely $k_v = 10^6$ N/m and $k_v = 10^7$ N/m. Notably, the impact factor exhibits contrasting trends depending on the suspension stiffness. For the lower stiffness case ($k_v = 10^6$ N/m), the impact factor decreases with increasing m_1, whereas for

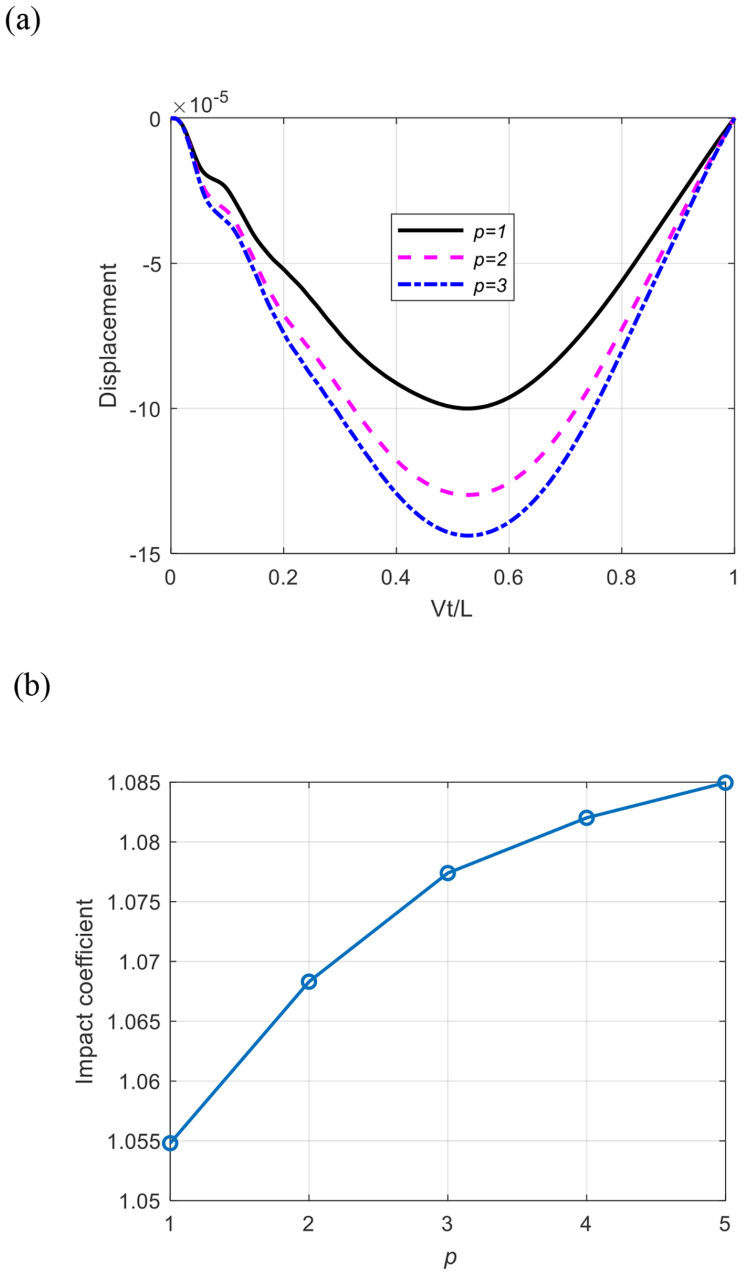

Figure 3. The effects of the power-law index p on displacement (a) and impact factor (b)

the higher stiffness case ($k_v = 10^7$ N/m), the impact factor increases. This behavior is attributed to the dynamic interaction between the sprung mass and the beam. Specifically, when the suspension stiffness is relatively low, the vibration of m_1 may develop a phase lag relative to the beam response, which can attenuate the dynamic amplification. Conversely, a stiffer suspension transmits a greater proportion of the dynamic forces to the beam, thereby enhancing the amplification effect.

Influence of the moving load velocity

The effect of the vehicle travel velocity on the dynamic response was investigated in Figures 5 and 6. Figure 5 depicts the beam displacement time histories for various moving load velocities. As the load traverses the beam, the displacement initially increases in the negative direction, attaining a maximum near the mid-span region before gradually returning to zero as the load approaches the support. A clear trend is observed wherein the displacement amplitude increases along with velocity, with the case $v = 30$ m/s producing the largest deflection. This behavior indicates that higher travel speeds induce more pronounced dynamic effects.

Figures 6(a) and 6(b) present the impact factor as a function of the moving load velocity for two

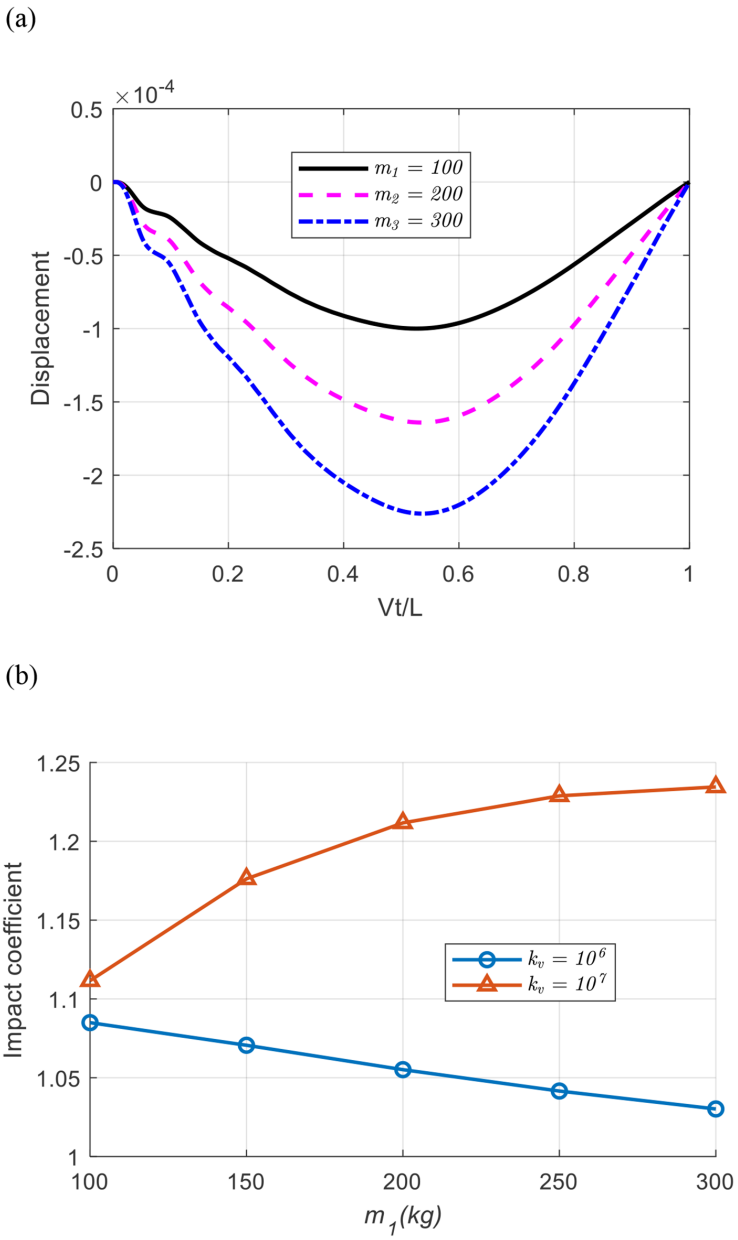

Figure 4. The effects of mass m_1 on displacement (a) and impact factor (b)

suspension stiffness values, $k_v = 10^6$ N/m and $k_v = 10^7$ N/m, respectively. For each stiffness configuration, two damping conditions were examined: $c_v = 0$ (undamped) and $c_v = 10^4$ N · s/m (damped). The results revealed that the impact factor generally increases along with velocity; however, exceptions exist due to the complex nature of the vehicle–structure interaction. In certain parameter regimes, increasing the velocity may lead to a reduction in the impact factor, a phenomenon attributable to the phase lag between the inherent vibration of the moving vehicle and the beam deflection. A notable example of this behavior is observed in Figure 6(a) for the case $k_v = 10^6$ N/m and $c_v = 0$.

A comparison between Figures 6(a) and 6(b) further reveals that the impact factor is consistently larger for the higher suspension stiffness case ($k_v = 10^7$ N/m) across the range of velocities considered. This observation suggests that increasing the stiffness of the suspension system intensifies the dynamic coupling between the vehicle and the beam, thereby amplifying the overall dynamic response. The presence of damping ($c_v = 10^4$ N · s/m) generally attenuates the impact factor, particularly at higher velocities, underscoring the energy dissipation capacity of the suspension system.

The numerical results provide comprehensive insights into the dynamic interaction between a functionally graded beam and a two-degree-of-freedom moving vehicle. The validation example demonstrates that the proposed finite element formulation produces the results that are in excellent agreement with those obtained from the semi-analytical solution. The negligible discrepancies between the two approaches confirm both the correctness of the developed element formulation and the reliability of the numerical implementation based on the Wilson–θ integration scheme. This agreement validates the capability of the proposed computational framework to accurately capture the transient vibration response of the FGM beams subjected to moving vehicle loads.

The parametric investigation revealed that the material gradation represented by the power-law index significantly influences the dynamic response of the beam. As the power-law index increases, the metallic volume fraction becomes larger, which reduces the effective bending stiffness of the FGM beam. Consequently, the structure becomes more flexible and exhibits larger mid-span deflections under moving loads. This stiffness reduction also results in a noticeable increase in the dynamic amplification factor. These observations indicate that the distribution of constituent materials in FGM beams plays an important role in controlling their dynamic performance and should therefore be carefully considered during structural design.

The results also highlight the important role of the moving vehicle mass in the coupled vehicle–beam interaction. Increasing the moving mass naturally raises the magnitude of the excitation acting on the beam, which leads to larger displacement responses. However, the influence on the dynamic amplification factor

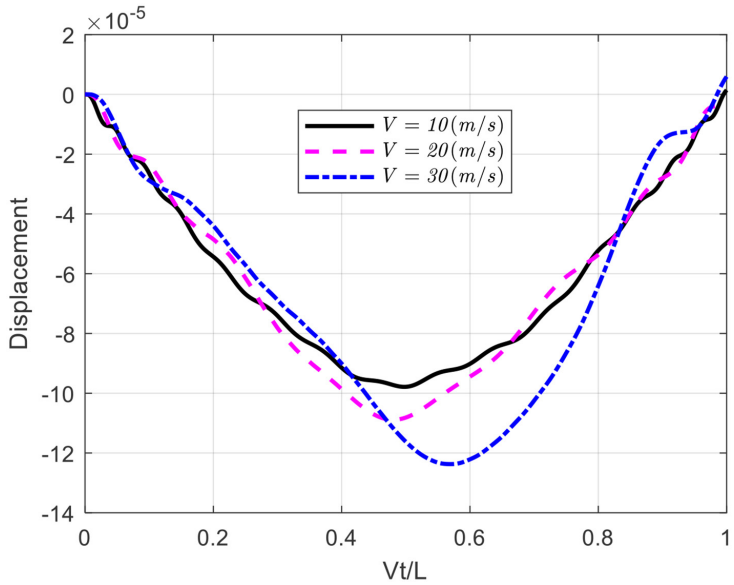

Figure 5. Effect of the moving load velocity on displacement

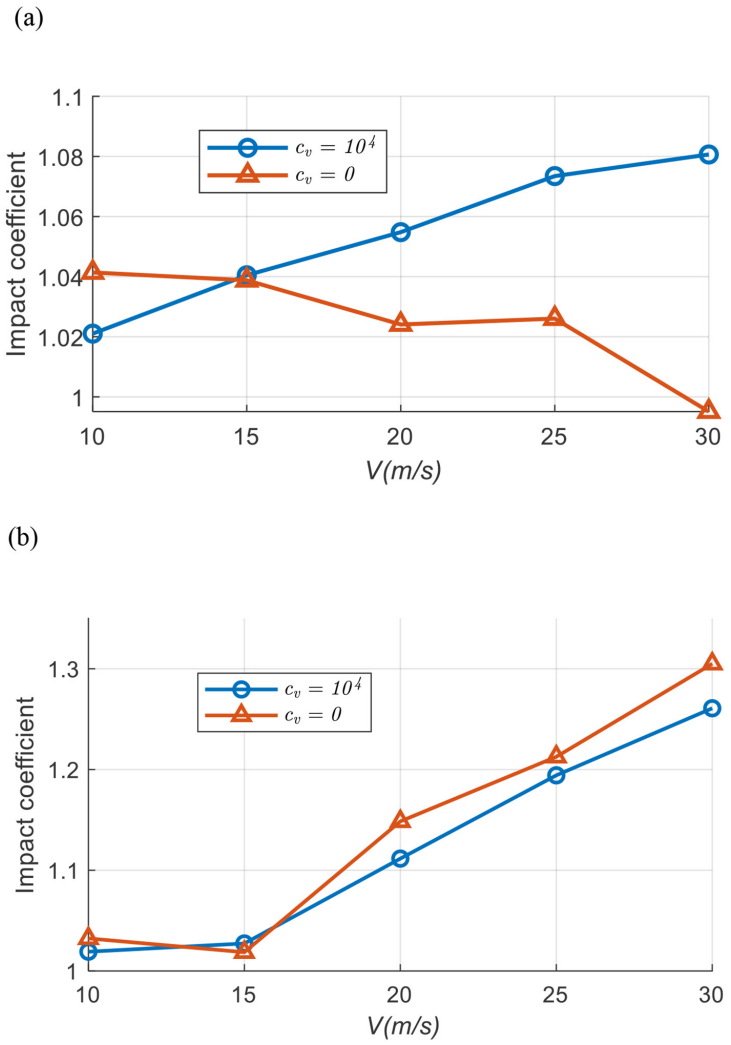

Figure 6. Effect of velocity of moving load impact factor: (a) k_v = 10⁶ N/m; (b) k_v = 10⁷N/m

depends strongly on the stiffness of the suspension system connecting the two masses of the moving vehicle. When the suspension stiffness is relatively low, increasing the moving mass may reduce the impact factor due to the phase lag between the vehicle vibration and the beam response. In contrast, when the suspension stiffness becomes larger, the vehicle behaves more rigidly and transmits a greater portion of its dynamic energy to the beam, which leads to an increase in the impact factor. This behavior clearly illustrates the importance of considering the coupled dynamics of the vehicle–structure system rather than modeling the load as a simple moving force.

The travelling velocity of the moving load is another key parameter governing the vibration behavior of the system. In general, increasing the velocity leads to larger displacement amplitudes and higher dynamic amplification factors. This occurs because higher travelling speeds intensify the dynamic excitation acting on the structure. When the excitation frequency associated with the moving vehicle approaches the natural vibration characteristics of the beam, stronger dynamic responses can occur. Nevertheless, due to the coupled dynamics between the beam and the moving vehicle, certain velocity ranges may produce a reduction in the dynamic amplification factor. This phenomenon is associated with the phase difference between the vibration of the moving load and the beam response, which can partially reduce the dynamic interaction effect.

The suspension characteristics of the moving vehicle, including stiffness and damping, also affect the vibration behavior of the system. Increasing the suspension stiffness tends to enhance the transmission of dynamic forces from the vehicle to the beam, resulting in larger impact factors. Conversely, the presence of

damping in the vehicle suspension can dissipate vibration energy and mitigate dynamic amplification to some extent. These findings highlight the complex nature of vehicle–structure interaction and demonstrate that both structural parameters and vehicle characteristics must be considered simultaneously to obtain accurate predictions of dynamic responses.

Overall, the present results indicate that the dynamic behavior of the functionally graded beams subjected to moving vehicle loads is governed by a complex interaction between material gradation, vehicle mass, suspension characteristics, and travelling velocity. The finite element framework developed in this study provides an effective tool for analyzing such coupled dynamic systems and offers useful insights for the design and optimization of beam-type structures in transportation and bridge engineering applications.

To address the need for a deeper analysis of parameter influences and to identify engineeringly significant regimes, the sensitivity of the dynamic response across the full range of each parameter was systematically examined. The results reveal that the power-law index p exerts a substantial influence on the impact factor (IF), with IF increasing nearly linearly by approximately 28% as p rises from 1 to 5. This indicates that material gradation is a critical design factor when dynamic amplification is a concern. Regarding the moving load velocity, the displacement amplitude increases by up to 58% when v increases from 10 m/s to 30 m/s, with the most pronounced sensitivity observed for stiffer suspension systems ($k_v = 10^7$ N/m). From an engineering standpoint, this suggests that for high-speed railway bridges, velocity control or enhanced damping may be necessary to mitigate excessive vibrations. Conversely, for softer suspension systems ($k_v = 10^6$ N/m), the impact factor does not increase monotonically with velocity; instead, a reduction in IF is observed in certain velocity ranges due to phase lag between the vehicle oscillation and the beam deflection. This non-monotonic behavior implies that simply reducing vehicle speed does not always guarantee lower dynamic amplification. Finally, increasing the sprung mass m_1 from 100 kg to 300 kg leads to a 35–38% increase in displacement, but its effect on IF depends strongly on suspension stiffness: IF decreases by about 12% when k_v is low, whereas it increases by about 18% when k_v is high. This contrasting trend highlights that the coupled dynamics of the vehicle–structure system must be considered as a whole, rather than treating the moving load as an independent forcing function.

Before concluding, it is important to acknowledge certain limitations of the proposed model. First, the use of Euler–Bernoulli beam theory assumes that plane sections remain plane and perpendicular to the neutral axis after deformation, which is valid only for slender beams with a length-to-thickness ratio $L/h > 20$. For thicker FGM beams where shear deformation becomes significant, higher-order shear deformation theories (HSDTs) or Timoshenko beam theory would be more appropriate. Second, the moving vehicle is idealized as a two-degree-of-freedom oscillator that maintains continuous contact with the beam. This assumption neglects the possible loss of contact (separation) between the vehicle and the beam, which may occur under high-speed or rough surface conditions, as well as longitudinal and lateral vehicle dynamics. Third, the material gradation follows a simple power-law distribution, whereas real FGM structures may exhibit more complex porosity distributions or bidirectional gradations. Despite these simplifications, the present model captures the essential physics of the vehicle–FGM beam interaction and provides a reliable foundation for more refined analyses. Extending the current framework to include shear deformation, contact loss, and more sophisticated material models constitutes a promising direction for future research.

The influence of suspension stiffness and damping observed in Figures 4(b) and 6 carries important practical implications for bridge design. For high-speed railway bridges, where the suspension system of trains is typically stiff (k_v on the order of 10^7 N/m) to maintain stability, the dynamic amplification factor (IF) increases with both vehicle speed and sprung mass. This implies that, for such bridges, speed limits may be necessary to prevent excessive vibrations, or alternatively, additional damping devices should be incorporated into the bridge structure to compensate for the limited energy dissipation capacity of the stiff suspension. In contrast, for pedestrian bridges or low-speed overpasses, where vehicles often have softer suspension systems ($k_v \approx 10^6$ N/m), increasing the vehicle mass can actually reduce the IF due to phase lag effects, as shown in Figure 4(b). This counterintuitive finding suggests that for such structures, heavier vehicles do not necessarily cause proportionally

larger dynamic amplification, which may be considered in load rating and design codes. Furthermore, the presence of damping (c_v = 10⁴ N·s/m) consistently reduces the IF, particularly at higher velocities (Figure 6), confirming that well-maintained suspension systems contribute not only to ride comfort, but also to reduced dynamic loading on the bridge. These insights highlight that the accurate prediction of vehicle–bridge interaction requires careful consideration of suspension characteristics, and that simplified moving load models may lead to either overly conservative or unsafe designs, depending on the specific vehicle and bridge parameters.

CONCLUSIONS

The present study successfully developed a finite element formulation for the dynamic analysis of functionally graded beams based on the classical beam theory, considering a two-degree-of-freedom moving load model. A MATLAB computational program was successfully implemented according to the derived finite element equations and integrated with the Wilson–θ algorithm to evaluate the vibration responses of the beam.

In addition, a semi-analytical approach combined with the Wilson–θ scheme was established to compute the dynamic responses for validation purposes. The comparison between the finite element results and the semi-analytical solutions shows excellent agreement, with only negligible discrepancies, thereby confirming the accuracy and reliability of the proposed finite element formulation.

Parametric studies were conducted to investigate the influence of various beam and moving load parameters. Within the range of data considered in this study, the following observations can be drawn:

Increasing the gradient index of the material volume fraction reduces the effective bending stiffness of the beam, leading to larger dynamic displacements and higher dynamic amplification factors.

When the moving mass m_1 increases from 100 to 300 kg, the dynamic amplification factor increases for larger stiffness values k_v, whereas it decreases when k_v is smaller.

As the velocity increases from 10 to 30 m/s, the beam tends to exhibit stronger dynamic responses, leading to larger displacements and higher dynamic amplification factors. However, in some cases, the dynamic amplification factor may decrease due to the phase lag associated with the moving load.

Stiffer suspension systems transmit more dynamic energy to the beam, resulting in larger IF values, while the presence of damping (c_v= 10⁴ N · s/m) consistently reduces the IF, particularly at higher velocities.

The study acknowledges certain limitations, including the use of Euler–Bernoulli beam theory (valid only for slender beams with L/h>20), the assumption of continuous contact between the vehicle and the beam, and the simple power-law material distribution. Extending the framework to include shear deformation, contact loss, and more complex material gradations is a promising direction for future research.

These findings provide valuable insights into the dynamic behavior of functionally graded beams subjected to moving loads and demonstrate the effectiveness of the proposed computational framework.

REFERENCES

1. Al-Ashtari W., A new approach for modelling the vibration of beams under moving load effect, ARPN J. Eng. Appl. Sci, 2023; 18: 1195–1206.
2. Khalili S.M.R., Jafari A.A., Eftekhari S.A., A mixed Ritz-DQ method for forced vibration of functionally graded beams carrying moving loads, Composite Structures, 2010; 92: 2497–2511. https://doi.org/10.1016/j.compstruct.2010.02.012
3. Şimşek M., Vibration analysis of a functionally graded beam under a moving mass by using different beam theories, Composite Structures, 2010; 92: 904–917. https://doi.org/10.1016/j.compstruct.2009.09.030
4. Şimşek M., Kocatürk T., Free and forced vibration of a functionally graded beam subjected to a concentrated moving harmonic load, Composite Structures, 2009; 90: 465–473. https://doi.org/10.1016/j.compstruct.2009.04.024
5. Hirzinger B., Adam C., Salcher P., Dynamic response of a non-classically damped beam with general boundary conditions subjected to a moving mass-spring-damper system, International Journal of Mechanical Sciences, 2020; 185: 105877. https://doi.org/10.1016/j.ijmecsci.2020.105877
6. Rajabi K., Kargarnovin M.H., Gharini M., Dynamic analysis of a functionally graded simply supported Euler–Bernoulli beam subjected to a moving oscillator, Acta Mechanica, 2013; 224: 425–446. https://doi.org/10.1007/s00707-012-0769-y

7. Chung N.T., Hong N.T., Thuy L.X., Dynamic analysis of cracked plate subjected to moving oscillator by finite element method, Mathematical Problems in Engineering, 2019; 2019: 6528251. https://doi.org/10.1155/2019/6528251
8. Vu A.N.T., Nguyen D.K., Nonlinear dynamics of two-directional functionally graded beam under a moving load with influence of homogenization scheme, Journal of Vibration Engineering & Technologies, 2024; 12: 171–185. https://doi.org/10.1007/s42417-024-01409-w
9. Guendouz I., Vidal P., Khebizi M., Guenfoud M., Advanced numerical free vibration analysis of FG thin-walled i-beams using refined beam models, Journal of Composites Science, 2025; 19.
10. Mashat D.S., Carrera E., Zenkour A.M., Al Khateeb S.A., Filippi M., Free vibration of FGM layered beams by various theories and finite elements, Composites Part B: Engineering, 2014; 59: 269–278. https://doi.org/10.1016/j.compositesb.2013.12.008
11. Mokhtar E., Mashhour A.A., Mokhtar B., Mohamed A.E., Noureddine B., Effects of changing materials properties for vibration of FGM beam using integral shear deformation model, Coupled systems mechanics, 2024; 13: 277–291. https://doi.org/10.12989/csm.2024.13.4.277
12. Alshorbagy A.E., Eltaher M.A., Mahmoud F.F., Free vibration characteristics of a functionally graded beam by finite element method, Applied Mathematical Modelling, 2011; 35: 412–425. https://doi.org/10.1016/j.apm.2010.07.006
13. Elhannani A., Brahami R., Elmeiche A., Bouamama M., Rabehi A., Benghanem M., Analytical investigation of free vibrations in functionally graded material beams with different property distributions, Nigerian Journal of Technological Development, 2025; 22: 240–249. https://doi.org/10.63746/njtd.v22i3.3530
14. Sina S.A., Navazi H.M., Haddadpour H., An analytical method for free vibration analysis of functionally graded beams, Materials & Design, 2009; 30: 741–747. https://doi.org/10.1016/j.matdes.2008.05.015
15. Su H., Banerjee J.R., Cheung C.W., Dynamic stiffness formulation and free vibration analysis of functionally graded beams, Composite Structures, 2013; 106: 854–862. https://doi.org/10.1016/j.compstruct.2013.06.029
16. Thai H.-T., Vo T.P., Bending and free vibration of functionally graded beams using various higher-order shear deformation beam theories, International Journal of Mechanical Sciences, 2012; 62: 57–66. https://doi.org/10.1016/j.ijmecsci.2012.05.014
17. Burlayenko V.N., Kouhia R., Dimitrova S.D., One-Dimensional vs. three-dimensional models in free vibration analysis of axially functionally graded beams with non-uniform cross-sections, Mechanics of Composite Materials, 2024; 60: 83-102. https://doi.org/10.1007/s11029-024-10176-4
18. Malekzadeh P., Karami G., Out-of-plane static analysis of circular arches by DQM, International Journal of Solids and Structures, 2003; 40: 6527–6545. https://doi.org/10.1016/S0020-7683(03)00412-8
19. Ghayesh M.H., Resonant dynamics of axially functionally graded imperfect tapered Timoshenko beams, Journal of Vibration Control, 2019; 25: 336–350.
20. El Hantati I., Outassafte O., El Khouddar Y., Belhaou M., Adri A., Benamar R., Analysis of the transverse vibration of a multistepped FGM beam resting on a Winkler foundation in a thermal environment and carrying concentrated masses, Results in Engineering, 2024; 23: 102822. https://doi.org/10.1016/j.rineng.2024.102822
21. Eltaher M.A., Emam S.A., Mahmoud F.F., Free vibration analysis of functionally graded size-dependent nanobeams, Applied Mathematics and Computation, 2012; 218: 7406–7420. https://doi.org/10.1016/j.amc.2011.12.090
22. Vu A.N.T., Nguyen D.K., Size-dependent transient response of sandwich microbeam with three-phase bidirectional FGM face layers under a moving mass, Archive of Applied Mechanics, 2024; 94: 2101–2122. https://doi.org/10.1007/s00419-024-02628-z
23. Nguyen D.K., Thom T.T., Gan B.S., Van Tuyen B., Influences of dynamic moving forces on the functionally graded porous-nonuniform beams, International Journal of Engineering Technology Innovation, 2016; 6: 173.
24. Nguyen V.-L., Tran M.-T., Chu T.-B., Nguyen T.-A., Nguyen V.-L., Nonlinear dynamic response of functionally graded porous beams under a moving mass using Reddy's beam theory, Iranian Journal of Science and Technology, Transactions of Mechanical Engineering, 2024; 48: 1205–1221. https://doi.org/10.1007/s40997-023-00705-2
25. Gantayat A.K., Sutar M.K., Mohanty J.R., Pattnaik S., Analysis of free vibration characteristics of non-uniform graphene-reinforced axially functionally graded nanocomposite beam, Advanced Composite Materials, 2025; 34: 788–808. https://doi.org/10.1080/09243046.2024.2407956
26. Ke L.-L., Yang J., Kitipornchai S., Nonlinear free vibration of functionally graded carbon nanotube-reinforced composite beams, Composite Structures, 2010; 92: 676–683. https://doi.org/10.1016/j.compstruct.2009.09.024
27. Tran T.T., Esen I., Nguyen D.K., Dynamic behaviour of an inclined FG-CNTRC sandwich beam under a moving mass, Vietnam Journal of Science Technology, 2024; 62: 359–373. https://doi.org/10.15625/2525-2518/17174
28. Ellali M., Bouazza M., Zenkour A.M., Hygrothermal

vibration of FG nanobeam via nonlocal unknown integral variables secant-tangential shear deformation coupled theory with temperature-dependent material properties, European Journal of Mechanics - A/Solids, 2024; 105: 105243. https://doi.org/10.1016/j.euromechsol.2024.105243

29. Xu X., Wang Y., Vibration control of AFG beam with moving load in thermal environment, Materials, 2025; 725.
30. Jia S., Yang G., Pu Y., Ma P., Li K., Free vibration characteristics of functionally graded material (fgm) beams on three-parameter viscoelastic foundation, Journal of Composites Science, 2025; 215.
31. Zemri A., Mechab I., Finite element analysis of flexural, torsional, and vibrational behavior of functionally graded porous beams with bidirectional gradation, Mechanics Based Design of Structures and Machines, 2025; 1–26. https://doi.org/10.1080/15397734.2025.2568009
32. Bathe K.-J., Finite Element Procedures, Prentice-Hall, USA, 2014.
33. Paultre P., Dynamics of structures, John Wiley & Sons, USA, 2013.
34. Buntara S.G., Thanh-Huong T., Thi-Ha L., Dinh-Kien N., Dynamic response of non-uniform Timoshenko beams made of axially FGM subjected to multiple moving point loads, Structural Engineering and Mechanics, An Int' l Journal, 2015; 53: 981–995.
35. Nguyen D.K., Gan B.S., Le, T.H. Dynamic response of non-uniform functionally graded beams subjected to a variable speed moving load, Journal of Computational Science Technology, 2013; 7: 12–27.
36. Biswal A.R., Biswal D.R., vibrational energy harvesting from functionally graded nonprismatic beams, International Journal of Automotive Mechanical Engineering, 2025; 22: 12359–12372. https://doi.org/10.15282/ijame.22.2.2025.9.0946
37. Dao S.-D., Nguyen D.-D., Nguyen T.-H., Nguyen N.-L., An analytical solution for energy harvesting using a high-order shear deformation model in functionally graded beams subjected to concentrated moving loads, Modelling, 2025; 55.
38. Hien T.D., Thanh B.T., Quynh Giang N.T., Uncertainty qualification for the free vibration of a functionally graded material plate with uncertain mass density, IOP Conference Series: Earth and Environmental Science, 2018; 143: 012021. http://dx.doi.org/10.1088/1755-1315/143/1/012021
39. Duy H.T., Diem N.D., Van Tan G., Van Hiep V., Van Thuan N., Stochastic higher-order finite element model for the free vibration of a continuous beam resting on elastic support with uncertain elastic modulus, engineering, Technology Applied Science Research, 2023; 13: 9985–9990. https://doi.org/10.48084/etasr.5456
40. Ninh V.T.A., Fundamental frequencies of bidirectional functionally graded sandwich beams partially supported by foundation using different beam theories, Transport and Communications Science Journal, 2021; 72: 452–467. https://doi.org/10.47869/tcsj.72.4.5
41. Ninh V.T.A., Vibration of four-phase bidirectional functionally graded beams based on trigonometric enriched beam element, Transport and Communications Science Journal, 2025; 76: 965–979. https://doi.org/10.47869/tcsj.76.7.4
42. Tho N.C., Hoang V.V., Hai L.H., Ha N.H., Thao P.D., Tien D.M., Study of static bending of functionally graded beams using analytical method, Transport and Communications Science Journal, 2025; 76: 1049–1063. https://doi.org/10.47869/tcsj.76.7.1
43. Wilson E.L., Farhoomand I., Bathe K.J., Nonlinear dynamic analysis of complex structures, Earthquake Engineering & Structural Dynamics, 1972; 1: 241–252. https://doi.org/10.1002/eqe.4290010305
44. Taghipour A., Zakeri J.A., Mosayebi S.A., Investigations on the effects of rail longitudinal forces in train-track dynamic interaction, Periodica Polytechnica Civil Engineering, 2024; 68: 364– https://doi.org/374.10.3311/PPci.22964
45. Diem N.D., Van Dat P., Hien T.D., Analysis of beams with a three-dimensional random field of the modulus of elasticity using the stochastic finite element method, International Journal of Mathematical, Engineering and Management Sciences, 2025; 10: 1518–1538. https://doi.org/10.33889/IJMEMS.2025.10.5.072
46. Abdulkhudhur R., Dawood H., Al-Quraishi, H.M., Numerical investigation for selection the optimal flexural strengthening strategy of reinforced concrete beams. Civil Engineering Journal, 2025; 11(10): 4281–4292. https://doi.org/10.28991/CEJ-2025-011-10-016
47. Su, J., Lai, Q., Hu, J., Xu, L., Xie, L., Zou, Y. Optimization of the ground motion intensity measure for long-span suspension bridges considering the impulse effect. HighTech and Innovation Journal, 2025; 6(1): 91–103. https://doi.org/10.28991/HIJ-2025-06-01-07
48. Mohammed, S. D., Salman, H. M., Ibrahim, T. H., Oukaili, N. K., Allawi, A. A. On the impact of lacing reinforcement arrangement on reinforced concrete deep beams performance. Civil Engineering Journal, 2025; 11(2): 726–745. https://doi.org/10.28991/CEJ-2025-011-02-019